Supporting Information

Chemical Evolution in Silicon-Graphite Composite Anodes Investigated by Vibrational Spectroscopy

Rose E. Ruther[a,*] , Kevin A. Hays[a], Seong Jin An[a,b], Jianlin Li[a,b], David L. Wood[a,b], and Jagjit Nanda[a,b,*]

[a]Oak Ridge National Laboratory, Oak Ridge, TN 37831 USA

[b]Bredesen Center for Interdisciplinary Research and Graduate Education, University of Tennessee, Knoxville, TN 37996, USA

[*]*Corresponding Authors:*
E-mail address: rutherre@ornl.gov. Telephone:(865)946-1578
E-mail address: nandaj@ornl.gov. Telephone:(865)241-8361

Anode Rinsing Procedure

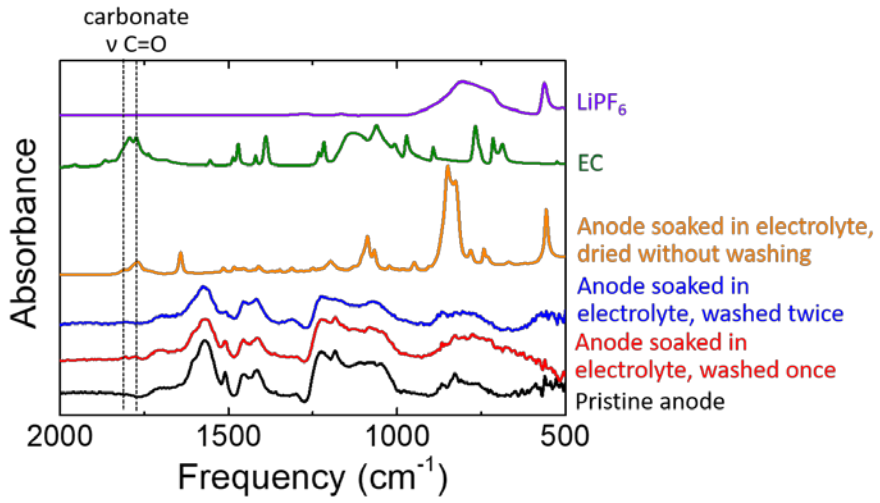

Figure S1. Evaluation of the effectiveness of rinsing the electrodes in DMC to remove excess electrolyte. FTIR spectra are shown for a pristine anode, an anode soaked in electrolyte and washed for 5 minutes in DMC once, an anode soaked in electrolyte and washed for 5 minutes in DMC twice, and an anode soaked electrolyte and dried without washing. FTIR spectra of pure EC and pure $LiPF_6$ are shown for reference.

Before collecting FTIR on cycled electrodes, excess electrolyte is typically removed by rinsing in a pure solvent such as DMC. However, the washing procedure can also remove components of the SEI, and aggressive rinsing procedures are generally avoided.[1-2] As a simple control experiment to test the effectiveness of the rinsing procedure, uncycled anodes were soaked in electrolyte and washed with pure DMC for 5 minutes once and twice. FTIR spectra were collected on the anodes after washing (**Figure S1**). While most of the electrolyte is removed after 5 minutes in DMC, two small bands near 1800 cm^{-1} are attributed to the carbonate stretch in residual EC. The EC is completely removed after washing for a second time for five minutes in fresh DMC. Therefore, two 5-minute washes were adopted as the standard rinsing procedure for cycled anodes.

Laser Power Study

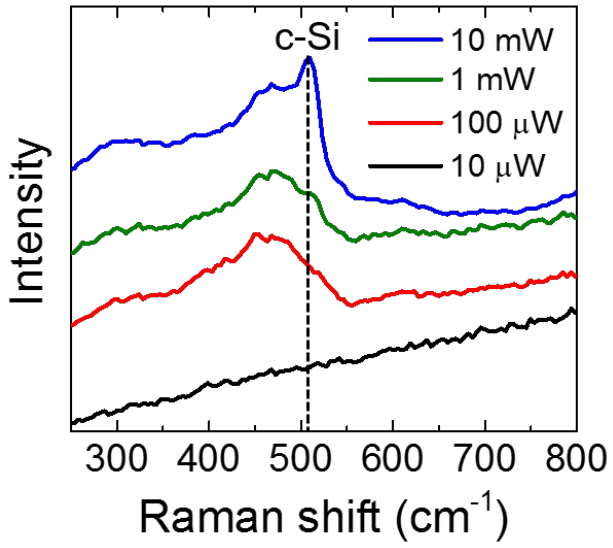

Figure S2. Raman spectra taken from the same location on a cycled Si-Gr anode with increasing laser power.

To minimize damage from laser-induced heating, Raman maps were collected with the lowest practical laser power of 100 μW (**Figure S2**). No signals from Si were observed if the laser power was attenuated further to 10 μW. High laser power (≥10 mW) caused the a-Si to partially crystallize, as indicated by the emergence of the sharp band near 510 cm^{-1} (**Figure 7**). The crystallization temperature for a-Si is typically 600-700 °C.[3-6]

Cycling Performance of NMC532 Cathode and Si-Gr Anode in Half Cells

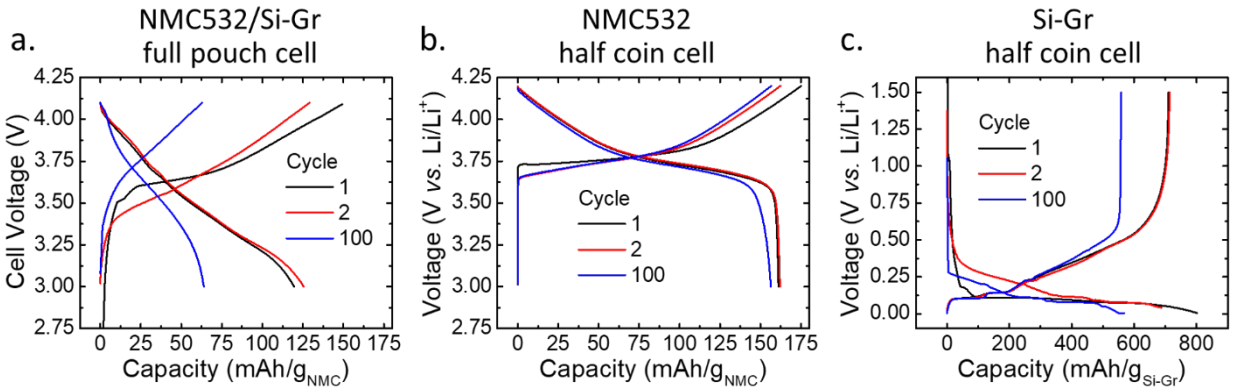

Figure S3. Voltage profiles during cycles 1,2, and 100 for (a) NMC532/Si-Gr full cell cycled between 3.0 and 4.1 V (b) NMC532 half cell with lithium metal counter electrode cycled between 3.0 and 4.2 V and (c) Si-Gr composite half cell with lithium metal counter electrode cycled between 0.005 and 1.5 V. The cycling protocol for the half cells was similar to the full cells without the DC resistance test. The half cells underwent 3 formation cycles at C/20 charge and discharge rates, 94 aging cycles at C/3 rate, and 3 final cycles at C/20 rate.

Raman and XRD of NMC532 Cathode after 100 Cycles in the Full Cell

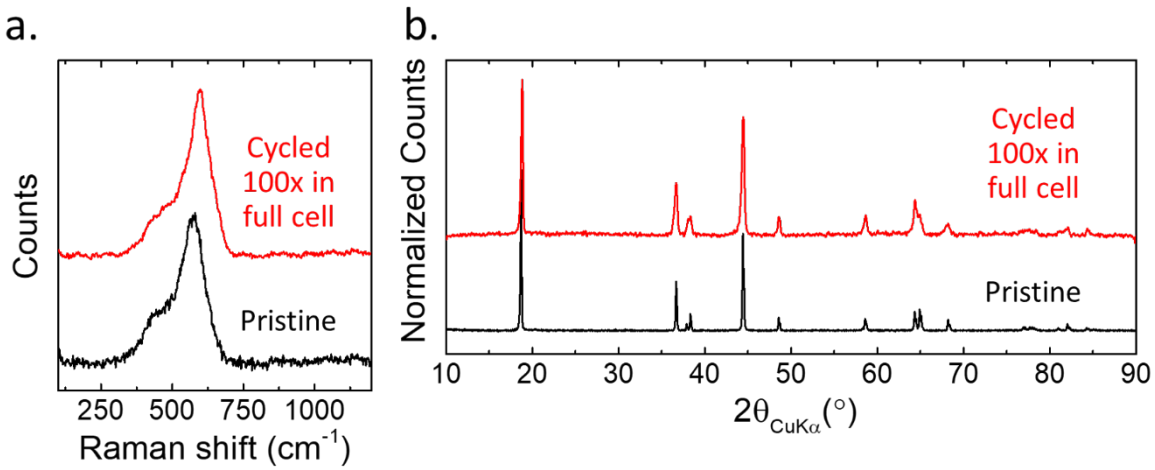

Figure S4. Characterization of the structure of the NMC532 cathode before and after 100 cycles in the full pouch cell. For comparison, the cycled cathode was fully discharged in a half cell with a lithium metal counter electrode prior to analysis. (a) Raman spectra. (b) XRD patterns.

Polymer-Binder Interactions

Binders with carboxylic acid or carboxylate groups tend to perform better in silicon anodes, which is often attributed to strong interactions between these functional groups and the surface of the

silicon particles.[7-10] Various interactions have been described including hydrogen bonding[9] and the formation of ester-type bonds with the Si surface.[8] Surface adsorption of polyacrylic acid and polyacrylates is typically accompanied by shifts in the position of the carboxylate modes.[11-13] No significant shifts in these modes are observed when comparing pure LiPAA to the composite anode (**Figure 3**). However, the fraction of LiPAA binder (10 wt.%) in the composite anode is large relative to the available surface area of the other solids, and most of the carboxylate groups cannot bind to any surface. If all the available surface area in the fully delithiated anode were uniformly covered with LiPAA, the polymer film would be around 15 nm thick. Alternatively, there are approximately 100 carboxylate groups per nm^2 of surface area, which is much greater than the number of carboxylic acid groups in a close-packed monolayer film (~ 5 $COOH/nm^2$).[14] Due to the relatively small fraction of polymer that can interact with the surface, silicon-binder interactions are difficult to probe in these electrodes.

Anode Washing After 100 Cycles

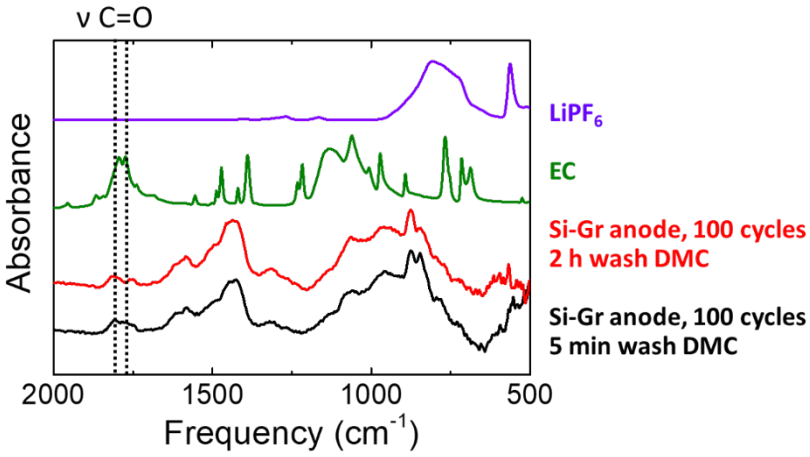

Figure S5. FTIR spectra of Si-Gr anodes cycled 100 times and rinsed 5 min in DMC and 2 h in DMC. FTIR spectra of pure EC and pure $LiPF_6$ are shown for reference. EC is not removed even after 2 h in DMC, suggesting EC is trapped in a thick SEI layer that forms after 100 cycles.

Comparison of SEI that Forms in Full and Half Cells

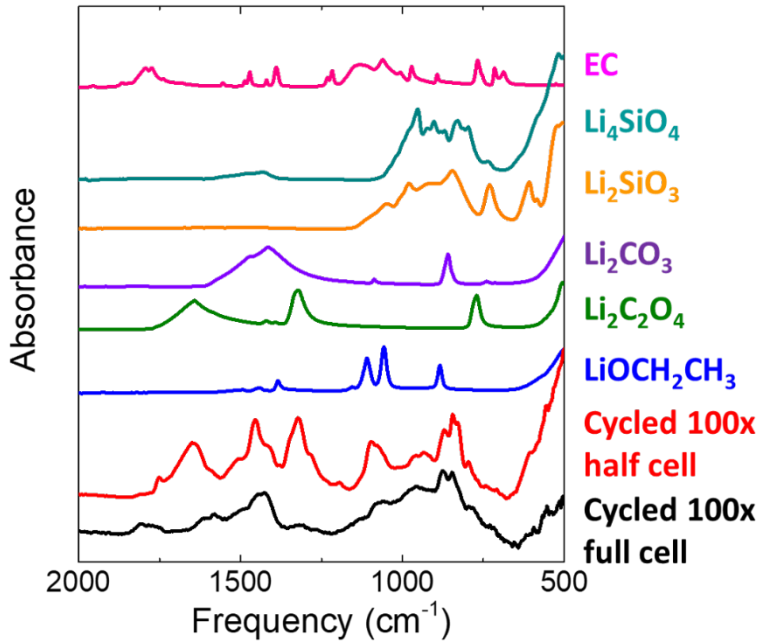

Figure S6. FTIR spectra of Si-Gr anodes after 100 cycles in a full pouch cell with an NMC532 cathode and 100 cycles in a half coin cell with a lithium metal counter electrode. FTIR spectra of $LiOCH_2CH_3$, $Li_2C_2O_4$, Li_2CO_3, Li_2SiO_3, Li_4SiO_4, and EC are also shown for comparison.

Uniformity of c-Si to a-Si Phase Transition for Anodes Cycled in Full and Half Cells

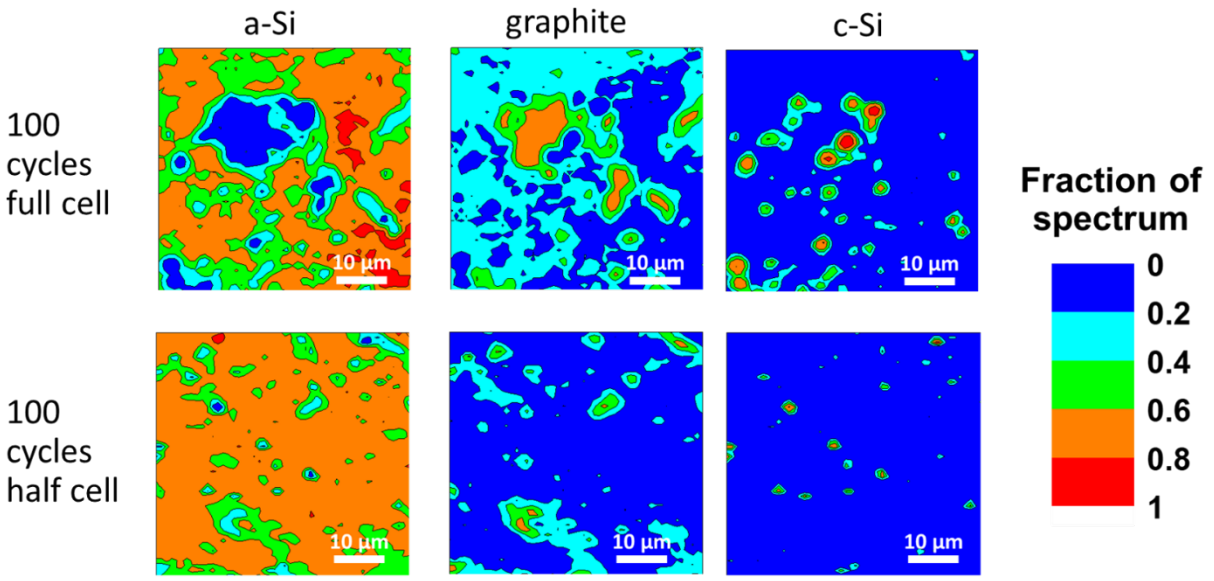

Figure S7. Raman maps of Si-Gr anodes after 100 cycles in a full pouch cell with an NMC532 cathode and 100 cycles in a half coin cell with a lithium metal counter electrode. Raman maps were generated by deconvoluting each spectrum into the sum of the four components shown in **Figure 7**. Small domains of crystalline silicon remain in both electrodes.

XRD Measurements of c-Si in Cycled Si-Gr Anodes

To verify that the presence of c-Si in the cycled electrodes was not an artifact of laser-induced heating, XRD was also collected **(Figure S8)**. The (002) diffraction peak of graphite serves as an internal standard to normalize the patterns and facilitate comparison. The (111) peak from c-Si decreases in intensity after cycling but does not disappear even after 100 cycles. The anode cycled twice shows less c-Si than the anode cycled once, indicating that there is some cell-to-cell variation. Overall, the XRD confirms the results from Raman spectroscopy that some of the silicon does not participate in the alloy reaction with lithium and remains crystalline.

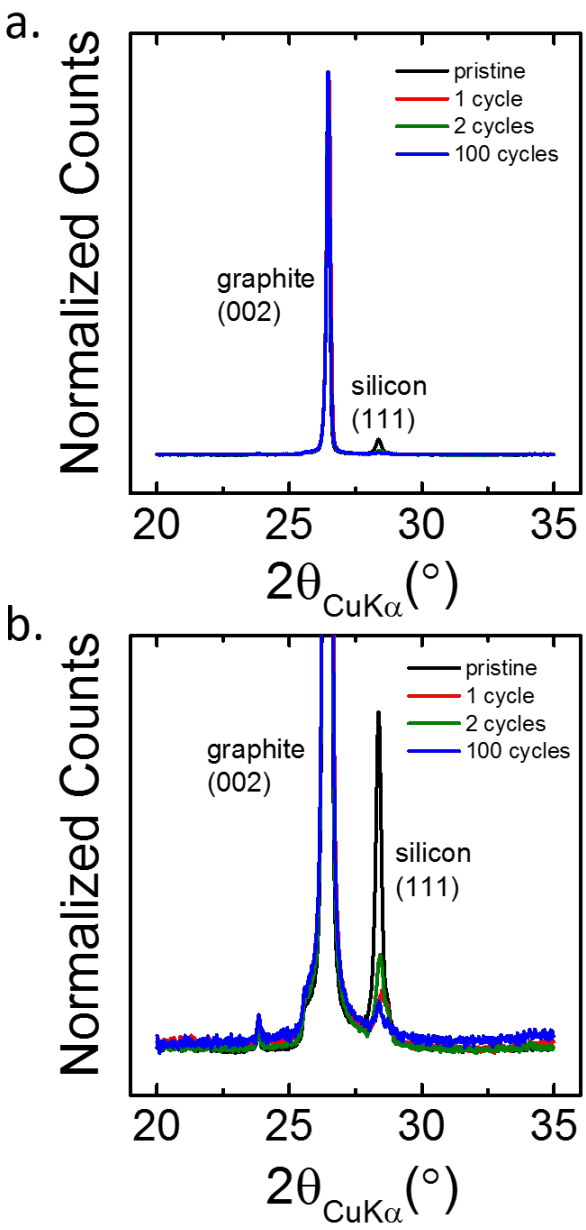

Figure S8. (a) XRD patterns of Si-Gr anodes before and after cycling (b) Expanded view of the pattern shown in panel a to highlight the lower intensity peaks from Si (111).

References

1. Somerville, L.; Bareno, J.; Jennings, P.; McGordon, A.; Lyness, C.; Bloom, I., The Effect of Pre-Analysis Washing on the Surface Film of Graphite Electrodes. *Electrochim. Acta* **2016,** *206*, 70-76.

2. Waldmann, T.; Iturrondobeitia, A.; Kasper, M.; Ghanbari, N.; Aguesse, F.; Bekaert, E.; Daniel, L.; Genies, S.; Gordon, I. J.; Loble, M. W.; De Vito, E.; Wohlfahrt-Mehrens, M., Review-Post-Mortem Analysis of Aged Lithium-Ion Batteries: Disassembly Methodology and Physico-Chemical Analysis Techniques. *J. Electrochem. Soc.* **2016,** *163*, A2149-A2164.

3. Shen, T. D.; Koch, C. C.; McCormick, T. L.; Nemanich, R. J.; Huang, J. Y.; Huang, J. G., The Structure and Property Characteristics of Amorphous Nanocrystalline Silicon Produced by Ball-Milling. *J. Mater. Res.* **1995,** *10*, 139-148.

4. Poate, J. M., Some Thermodynamic Properties of Amorphous Si. *Nucl. Instr. Meth. Phys. Res.* **1983,** *209*, 211-217.

5. Donovan, E. P.; Spaepen, F.; Turnbull, D.; Poate, J. M.; Jacobson, D. C., Heat of Crystallization and Melting-Point of Amorphous-Silicon. *Appl. Phys. Lett.* **1983,** *42*, 698-700.

6. Nagasima, N.; Kubota, N., Crystallization of Amorphous Si Films Formed by Chemical Vapor-Deposition. *J. Vac. Sci. Technol.* **1977,** *14*, 54-56.

7. Klamor, S.; Schroder, M.; Brunklaus, G.; Niehoff, P.; Berkemeier, F.; Schappacher, F. M.; Winter, M., On the Interaction of Water-Soluble Binders and Nano Silicon Particles: Alternative Binder Towards Increased Cycling Stability at Elevated Temperatures. *Phys. Chem. Chem. Phys.* **2015,** *17*, 5632-5641.

8. Hochgatterer, N. S.; Schweiger, M. R.; Koller, S.; Raimann, P. R.; Wohrle, T.; Wurm, C.; Winter, M., Silicon/Graphite Composite Electrodes for High-Capacity Anodes: Influence of Binder Chemistry on Cycling Stability. *Electrochem. Solid State Lett.* **2008,** *11*, A76-A80.

9. Bridel, J. S.; Azais, T.; Morcrette, M.; Tarascon, J. M.; Larcher, D., Key Parameters Governing the Reversibility of Si/Carbon/CMC Electrodes for Li-Ion Batteries. *Chem. Mat.* **2010,** *22*, 1229-1241.

10. Jeena, M. T.; Lee, J. I.; Kim, S. H.; Kim, C.; Kim, J. Y.; Park, S.; Ryu, J. H., Multifunctional Molecular Design as an Efficient Polymeric Binder for Silicon Anodes in Lithium-Ion Batteries. *ACS Appl. Mater. Interfaces* **2014,** *6*, 18001-18007.

11. Zaman, A. A.; Tsuchiya, R.; Moudgil, B. M., Adsorption of a Low-Molecular-Weight Polyacrylic Acid on Silica, Alumina, and Kaolin. *J. Colloid Interface Sci.* **2002,** *256*, 73-78.

12. Kirwan, L. J.; Fawell, P. D.; van Bronswijk, W., In Situ FTIR-ATR Examination of Poly(Acrylic Acid) Adsorbed onto Hematite at Low pH. *Langmuir* **2003,** *19*, 5802-5807.

13. Hu, H.; Saniger, J.; Garciaalejandre, J.; Castano, V. M., Fourier-Transform Infrared-Spectroscopy Studies of the Reaction Between Polyacrylic-Acid and Metal-Oxides. *Mater. Lett.* **1991,** *12*, 281-285.

14. Allara, D. L.; Nuzzo, R. G., Spontaneously Organized Molecular Assemblies .1. Formation, Dynamics, and Physical-Properties of Normal-Alkanoic Acids Adsorbed from Solution on an Oxidized Aluminum Surface. *Langmuir* **1985,** *1*, 45-52.